InxGa1-xN/GaN double heterojunction solar cell optimization for high temperature operation

Bilel Chouchen, Frédérique Ducroquet, Samia Nasr, Abdullah Y.A. Alzahrani, Ali T Hajjiah, Mohamed Hichem Gazzah

$In_xGa_{1-x}N/GaN$ double heterojunction solar cell optimization for high temperature operation

Bilel. Chouchen[a], Frederique Ducroquet[b], Samia Nasr[c,d] , Abdullah Y.A. Alzahrani[e] , Ali T. Hajjiah[f*], Mohamed Hichem Gazzah[a]

[a]Quantum and Statistical Physics Laboratory, Faculty of Sciences of Monastir, University of Monastir, Monastir, 5019, Tunisia.
[b] Univ. Grenoble Alpes, Univ. Savoie Mont Blanc, CNRS, Grenoble INP, IMEP-LaHC, 38000 Grenoble, France
[c] Advanced Functional Materials & Optoelectronic Laboratory (AFMOL), Department of Physics, Faculty of Science, King Khalid University, P.O. Box 9004, Abha, Saudi Arabia.
[d] Electrochimie, Matériaux et Environnement (UREME [16ES02]), Institut préparatoire aux études d'ingénieurs Kairouan, Tunisia.
[e] Department of Chemistry, Faculty of Science and arts, King Khalid University, Mohail Assir, Abha, Saudi Arabia.
[f] Department of Electrical Engineering, College of Engineering and Petroleum, Kuwait University, Kuwait 13060, Kuwait

*corresponding author email(s): ali.hajjiah@ku.edu.kw, dr.hajjiah@gmail.com

Abstract

$In_xGa_{1-x}N/GaN$ solar cells are ideal candidates for use in extreme temperature applications. The conversion efficiency potential of double heterostructure solar cells was investigated at high temperatures using physical simulation. For a targeted working temperature, optimized efficiency lies in a compromise between the absorber bandgap energy determined by In composition and the band offsets at the heterointerface directly correlated with the capability for the photogenerated carriers to cross through the barrier by thermoionic emission. An optimized efficiency of 18% is obtained for an In content of 50% at 400K and decrease down to 10% for an In content of 35% at 500K. As the operating temperature goes higher, the indium content needs to be reduced in order to limit the detrimental effect of increasing intrinsic carrier concentration. The consequence is a decreasing efficiency due to the reduced covered range of the solar spectrum. In the same time, the band offsets are no more a limiting parameter, as there are reduced as the In content decreases, and as higher temperature increases the thermionic transport probability. This result shows the interest of $In_xGa_{1-x}N/GaN$ double heterostructure design for high temperatures applications.

Index Terms - InGaN, solar cell, high temperature, wide bandgap semiconductor

1. Introduction

New interest has recently been given to solar cells operating at high temperatures for their possible use in applications such as space missions [1], concentrated PV systems (CPV), photovoltaic/concentrated solar power (PV-CSP) hybrid system [2], hybrid solar thermal photovoltaic power plants, or optical power transmission [3]. The sensitivity to temperature of the efficiency is often expressed in terms of the normalized temperature coefficient [4]:

$$\frac{1}{\eta}\frac{\partial \eta}{\partial T} = \frac{1}{V_{OC}}\frac{\partial V_{OC}}{\partial T} + \frac{1}{J_{SC}}\frac{\partial J_{SC}}{\partial T} + \frac{1}{FF}\frac{\partial FF}{\partial T} \quad (1)$$

where V_{oc} is the open circuit voltage, J_{sc} the short circuit current, FF the fill factor and η the conversion efficiency. Fundamentally for most conventional solar cells, the intrinsic PV efficiency is found to decrease with increasing temperature [5]. The main contribution is the loss of V_{oc} due to an increase in the dark current. The decrease in bandgap with increasing temperature typically provides a small increase in $J_{SC,}$ the current variation being roughly proportional to the incident intensity at wavelengths near the band edges. For most cases the increase in J_{sc} is less than the decrease in V_{oc} resulting in a net decrease in performance as the temperature rises. However, the efficiency sensitivity is reduced for wide bandgap materials, increase of J_{sc} can be proportionally larger than the decrease of V_{oc} with temperature since the solar spectrum rapidly decreases at short wavelength near the band edge [1]. Therefore it was shown that optimum bandgap can be found as a function of operation temperature [6].

Among potential wide bandgap compounds for high temperature operations, the ternary $In_xGa_{1-x}N$ system has very promising properties. With bandgaps over a wide spectral region from 0.64eV (InN) to 3.4eV (GaN), full-spectrum-response multi-junction solar cells based solely on the III-Nitride materials were designed with near ideal bandgaps for maximum efficiency [7]. However, up to now, due to the degradation of crystalline quality with increasing In content caused by high lattice mismatched and InN segregation, the most promising applications remain confined to low In compositions, with therefore limited yields but of interest for extreme temperatures and harsh environment. Indeed, the InGaN alloys are one of few mature materials with direct bandgap greater than 2.5eV and offer high radiation resistance, strong absorption coefficient, as well as high carrier mobility, high drift velocity, high thermal conductivity and high temperature resistance [8].

Since the earliest report on InGaN based solar cells with clear PV response reported in 2007, fabrication of solar cells can be classified in two groups, the homojunction one including pin structures [9] and the heterojunction one including p-GaN/i-InGaN/n-GaN structures [7,10,11]. Detail review can be found in ref. [8]. However the best results are obtained on the heterojunctions, notably due to the difficulty to reach a high p-type doping level in InGaN [12]. A record-high In content of 22% was reported on such heterojunction structures [13]. When In content increases, the reduced bandgap of InGaN absorber improves the light absorption, leading to an increase of the conversion efficiency. However, when the indium composition further increases (larger than 20% at room temperature), the enlarged potential barrier height at the GaN/InGaN heterointerface can seriously degrade the carrier collection efficiency and consequently severely deteriorate the conversion efficiency [14].

In this paper, the efficiency potential of p^+-GaN/i-InGaN/n-GaN double heterojunction solar cells for high temperature operations are investigated using physical device simulation. An optimized indium composition is determined which depends on the targeted working temperature. Further improvements are discussed in terms of design and material parameters.

2. Simulation model

The Silvaco® device simulation tools software which was employed in this study self-consistency solves the Poisson equation and electron and hole current continuity equations [15]. The polarization charges caused by the spontaneous and piezoelectric polarization due to the wurtzite structure of InGaN are not taken into account in order to only focus on the effect of temperature. The physical parameter values used in the simulation are summarized in Table1.

II.1. Electrical and optical parameter properties depending on temperature

Bandgap energy:

The temperature dependence of the bandgap is given using the commonly used Varshni's law:

$$E_g^i(T) = E_g^i(0K) - \frac{\alpha T^2}{T+\beta} = E_g^i(300K) + \frac{\alpha \times 300^2}{300+\beta} - \frac{\alpha T^2}{T+\beta} \quad (2)$$

where *i* stands for InN or GaN, α and β are empirical parameters [16,17]. The $In_xGa_{1-x}N$ bandgap follows a simple quadratic form as a function of the In composition

$$E_g(x,T) = xE_g^{InN}(T) + (1-x)E_g^{GaN}(T) - bx(1-x) \quad (3)$$

where $E_g^{InN}$and E_g^{GaN} are the bandgap energies of InN and GaN, respectively and *b* is the bowing parameter for $In_xGa_{1-x}N$. The theoretical and experimental values of the bowing parameter are discussed in the literature and it was mainly found to depend on the state of the layer (stain or relaxed) and on the presence of In cluster. It was also suggested that value is dependent on the In composition, larger for low In composite [18] In this work we used a mean value of 1.65 corresponding to strained-free material as determined in [19]. Bandgap narrowing effects are not considered. A band discontinuity ratio ΔE_C:ΔE_V=70:30 is used for the GaN/InGaN heterojunction [20]

Low field mobility

The low field mobility is expressed following the expression proposed by Caughey-Thomas [21], depending on the carrier concentration N:

$$\mu_{e,h}(N) = \mu_{min_{e,h}} + \frac{(\mu_{max_{e,h}} - \mu_{min_{e,h}})}{1+\left(\frac{N}{N_{e,h}^{ref}}\right)^{\alpha_{e,h}}} \quad (4)$$

The temperature dependence of the mobility is obtained by modulating each parameter of eq. 4 by a factor $(T/300)^{\beta i}$ [22], leading to a formula close to that proposed by [23]:

$$\mu_{e,h}(T,N) = \mu_{min_{e,h}}\left(\frac{T}{300}\right)^{\beta 1_{e,h}} + \frac{\mu_{max_{e,h}}\left(\frac{T}{300}\right)^{\beta 2_{e,h}} - \mu_{min_{e,h}}\left(\frac{T}{300}\right)^{\beta 1_{e,h}}}{1+\left(\frac{N}{N_{e,h}^{ref}\left(\frac{T}{300}\right)^{\beta 3_{e,h}}}\right)^{\alpha_{e,h}\left(\frac{T}{300}\right)^{\beta 4}}} \quad (5)$$

Optical properties

Light absorption is described in the whole solar spectrum by the phenomenological model proposed in reference [27] where E_{ph} is the photon energy and with coefficients C and D extrapolated for all indium compositions by [28]:

$$\alpha = 10^5\sqrt{C\left(E_{ph} - E_g\right) + D(E_{ph} - E_g)^2} \quad (6)$$

The refractive index dispersion is given by the model proposed by Adachi [29] for phonon energies lower than the bandgap:

$$n(E) = \sqrt{a\left(\frac{E}{E_g}\right)^{-2}\left[2 - \sqrt{1+\frac{E}{E_g}} - \sqrt{1-\frac{E}{E_g}}\right] + b} \quad (7)$$

a and *b* are parameters dependent on the composition and for ternary compounds are obtained by linear interpolation with values given by [30]. Indeed due to the strong scattering of experimental data, the extraction of a bowing parameter is very difficult [30]. The imaginary portion of the refractive index is the extinction coefficient and is directly related to the absorption coefficient:

$$k(E) = \frac{\alpha(E)\,\lambda}{4\pi} \quad (8)$$

Radiative and non-radiative recombinations:

After electrons and holes are generated by photon absorption or thermally, they can be lost through a variety of recombination mechanisms which are temperature dependent processes. In this work, only radiative recombinations and non-radiative Shockley-Read-Hall (SRH) recombinations in the absorber are considered, other recombination processes as Auger or recombinations through interface states are not taken into account.

The radiative recombination rate can be written as:

$$R_{rad} = B(\mathrm{np} - \mathrm{n_i^2}) \quad (9)$$

where B is the radiative coefficient. Due to lack of data, the same value is considered on the whole In fraction. In p (n)-type GaN, the radiative minority carrier lifetime is given by $\tau_{rad} = (B \times n_0(p_0))^{-1}$ and is found increasing in proportion to the 1.5th power of temperature [32].

The Shockley Rad Hall recombination rate is given by:

$$\mathrm{R_{srh}}(cm^{-3}s^{-1}) = \frac{\mathrm{np} - \mathrm{n_i^2}}{\tau_{\mathrm{p}}^{\mathrm{srh}}\left[\mathrm{n} + \mathrm{n_i}.\exp\left(\frac{\mathrm{E_{trap}} - E_i}{\mathrm{kT}}\right)\right] + \tau_{\mathrm{n}}^{\mathrm{srh}}\left[\mathrm{p} + \mathrm{n_i}.\exp\left(\frac{E_i - \mathrm{E_{trap}}}{\mathrm{kT}}\right)\right]} \quad (10)$$

where $\tau_{\mathrm{n}}^{\mathrm{srh}}$ and $\tau_{\mathrm{p}}^{\mathrm{srh}}$ are the minority carrier lifetimes. $\mathrm{E_{trap}}$ is the position of the trap level from the intrinsic level. In this work $\mathrm{E_{trap}}$~0 close to $\mathrm{E_i}$ (mid-gap defect). The minority carrier lifetimes are given by:

$$\tau_{\mathrm{n,p}}^{srh} = \frac{1}{\sigma_{n,p}\, v_{th\ n,p} N_t^{srh}} \quad (11)$$

where N_t^{srh} is the concentration of non-radiative centers, $\sigma_{\mathrm{n,p}}$ are the capture cross-sections for electron and holes respectively and $\mathrm{v_{th\ n,p}}$ are the thermal velocities given by:

$$\mathrm{v_{thn,p}} = \sqrt{\frac{3\,\mathrm{k\,T}}{m_{n,p}^* m_0}} \quad (12)$$

The non-radiative minority carrier lifetime decreases with increasing temperature following $\mathrm{T^{-0.5}}$.

Charge transport

The carrier transport is modeled by standard drift-diffusion equations [15]. The transport over the heterointerfaces is taken into account using the thermionic field emission model [37].

In order to simplify the model, the tunneling contribution is neglected as only high temperature modeling are studied [37]. For the same reasons, the carrier confinement at the heterointerfaces is not considered [38]. The net electron and hole current density J_n and J_p crossing at the heterointerface from region 1 to region 2 are expressed by:

$$J_n = q\left(v_{n2}n_2(0^+) - v_{n1}n_1(0^-)exp\left(\frac{-\Delta Ec}{kT}\right)\right) \quad (13)$$

$$J_p = -q\left(v_{p2}p(0^+) - v_{p1}p(0^-)exp\left(\frac{-\Delta Ev}{kT}\right)\right) \quad (14)$$

where $n_1(0^-)$ and $n_2(0^+)$ ($p_1(0^-)$ and $p_2(0^+)$) are the electron (hole) densities at each side of the heterointerface and $v_{n1,2}$ and $v_{p1,2}$ are the mean electron and hole thermal velocities given by:

$$v_{n1,2} = \frac{A_n^* T^2}{qN_{c1,2}} \text{ and } v_{p1,2} = \frac{A_p^* T^2}{qN_{v1,2}} \quad (15)$$

with $N_{c1,2}$ ad $N_{v1,2}$ are the effective densities of states in the conduction and valence bands in region 1 and 2, respectively. $A^*_{n,p}$ is the effective Richardson constant for electrons, holes:

$$A^*_{n,p} = \frac{4\pi q k^2 m^*_{n,p} m_0}{h^3} \quad (16)$$

2.2. Structure

The InGaN/GaN p-i-n double heterojunction solar cell studied in the simulation is shown in Fig.1. The structure is composed of a 100nm thick n-type GaN bottom layer, an intrinsic $In_xGa_{1-x}N$ absorber layer and a 20nm thick p^+-GaN top layer. The residual doping of the non-intentionally doped InGaN layer is assumed to be 2×10^{16} cm^{-3}. The Si-doping concentration of the bottom layer is set at 5×10^{17} cm^{-3}. The p^+ region is obtained by Mg-doping concentration at 2×10^{19} cm^{-3}. The ionized donor and acceptor impurity concentrations are given by:

$$N_A^- = \frac{N_A}{1+g_A exp\left(\frac{E_A - E_F}{kT}\right)} \text{ and } N_D^+ = \frac{N_D}{1+g_D exp\left(\frac{E_F - E_D}{kT}\right)} \quad (17)$$

Due to the deep activation energy of the Mg acceptor, higher temperature allows more complete ionization of the impurities, which should have a beneficial effect to increase the electric field in the intrinsic absorber region [14]. N_t^{srh} is set at $10^{14}cm^{-3}$. The illumination employed in the simulation is the one sun AM1.5G solar spectrum at the top of the solar cell.

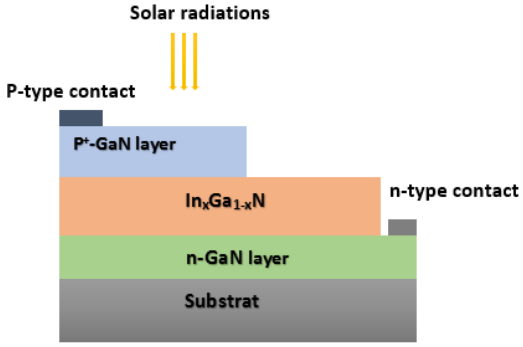

Fig.1: Schematic view of the double heterojunction GaN/$In_xGa_{1-x}N$/GaN pin solar cell.

Table I. Parameters used in numerical simulation for InN, GaN and $In_xGa_{1-x}N$.

Parameters	**GaN**	**InN**	**$In_xGa_{1-x}N$**
E_g(eV) à 0K	3.507 [16]	0.690 [17]	
α (eV/K)	0.909×10^{-3} [16]	0.414×10^{-3} [17]	
β (K)	830 [16]	454 [17]	
bowing parameter b			1.65 [19]
$\mu_{min,e}$ (cm^2/V.s)	80-100[22]	485[24]	
$\mu_{max,e}$ (cm^2/V.s)	1400[22]	10927[24]	
N^{ref}_e ($\times10^{17}cm^{-3}$)	0.8-1.6[22]	1.0[24]	
α_e	0.69-0.71[22]	0.6514[24]	
$\beta1_e$	-2.85[22]	-2.1948[24]	
$\beta2_e$	-0.2[22]	0.3997[24]	
$\beta3_e$	1.3[22]	1.3383[24]	
$\beta4_e$	0.31[22]	-0.5984[24]	
$\mu_{min,h}$ (cm^2/V.s)	0[25]	15[26]	
$\mu_{max,h}$ (cm^2/V.s)	31[25]	220[26]	
N^{ref}_h ($\times10^{18}cm^{-3}$)	18[25]	0.8[26]	
α_h	1.5[25]	1,25[26]	
$\beta1_h$	0	0	
$\beta2_h$	-2.5[25]	-2,5[26]	
$\beta3_h$	0	0	
$\beta4_h$	0	0	
μ(T,N)	μ_{GaN}(T,N)	μ_{InN}(T,N)	Linear interpolation
C	3.525 [27]	0.705	$3.525-18.29x+40.22x^2-37.52x^3+12.77x^4$ [28]
D	-0.6651 [27]	0,4909	$-0.6651+3.616x-2.46x^2$ [28]
a	10.1±0.3 [30]	9.4±0.5 [30]	Linear interpolation
b	2.67±0.08 [30]	5.0±0.2 [30]	Linear interpolation
B (cm^3/s)	$\sim5\times10^{-9}$ [31]	$\sim5\times10^{-9}$	constant with x
σ_n (cm^2)	5×10^{-13} [33]		
σ_p (cm^2)	7×10^{-14} [34]		
m^*_n	0.2[27]	0.05[27]	Linear interpolation
m^*_p	1.25[27]	0.42[35]	Linear interpolation
ε_r	8.9[27]	15.3[36]	Linear interpolation
E_d (meV)	12-17 [39] [Si]		
g_d	2[39] [Si]		
E_a (meV)	208[40] [Mg]: low doping level		
	118[41] [Mg]=$2\times10^{20}cm^{-3}$		

3. Results

3.1. Effects of the temperature and Indium content

Some works in the literature reported on the modelling of double heterojunction GaN/InGaN/GaN solar cells at room temperature [14,42,43]. The results show that the efficiency first increases when the In content increases due to the decrease of the bandgap which results in short circuit current increase. However, after reaching a maximum for In content around 0.2 and 0.3 depending on the design parameters of the structure (doping level, absorber thickness…)[14,42], the efficiency sharply drops for higher In content. When regarding the evolution of the energy band diagrams of InGaN/GaN p-i-n solar cell under equilibrium and 300K for different indium compositions (Fig. 2a-e), it can be seen that when the indium composition of $In_xGa_{1-x}N$ increases, the absorber bandgap decreases, inducing higher band offsets at the heterointerfaces with GaN. For In content of 0.1 and 0.2 (Figs. 2a and 2b), the electric field in the intrinsic layer enables the collect and the transport of the photogenerated carriers towards the electrodes. For In composition of 0.3 and higher (Fig 2c-e), the band offsets becomes sufficiently high to prevent the transport of the carriers from crossing into the contacts and the electric field in the intrinsic absorber becomes flat.

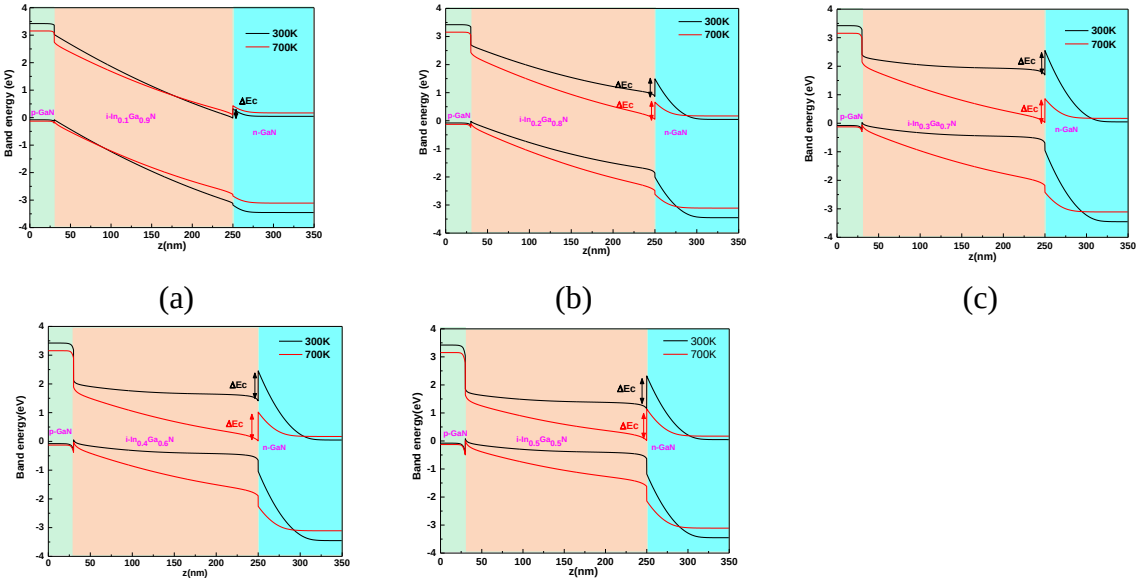

Fig.2: GaN/$In_xGa_{1-x}N$/GaN pin solar cell energy bandgap profile under zero bias at two temperatures 300K and 700K for various indium composition: (a) 0.1, (b) 0.2 (c) 0.3, (d) 0.4, (e) 0.5.

As observed on photocurrent versus voltage curve (Fig. 3a), the V_{oc} decreases as expected when the In content increases from 0.1 to 0.3 due to the reduction of the bandgap However, in the same time, although the number of photogenerated carriers is expected to increase due to the wider covered portion of the solar spectrum, J_{sc} is strongly reduced, due to the enlarged potential barrier height at the GaN/InGaN heterointerface. The photogenerated carriers cannot surmount the potential barrier by thermionic emission and consequently cannot be collected at the contacts and contribute to the photocurrent. The carrier lifetime is generally described as a competition between recombination and escape mechanisms [44] following:

$$\frac{1}{\tau} = \frac{1}{\tau_{rad}} + \frac{1}{\tau_{non\,rad}} + \frac{1}{\tau_{therm}} \qquad (18)$$

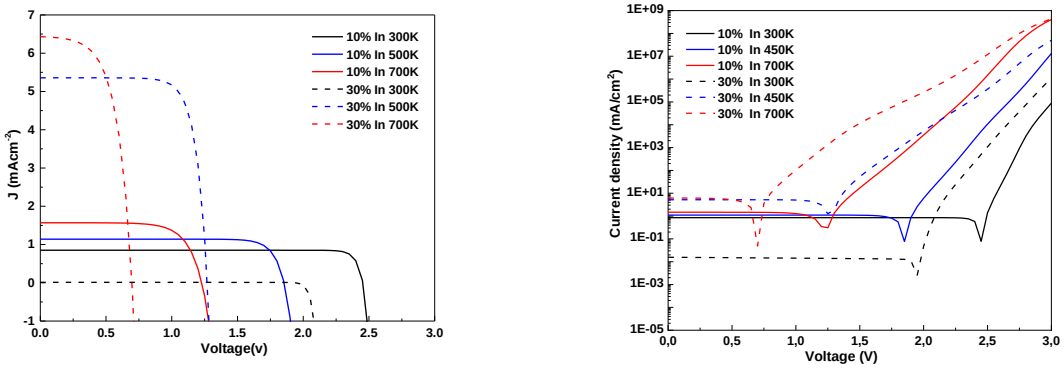

(a) (b)

Fig. 3 : Current-voltage characteristics for various temperatures and indium compositions. (a) – linear scale, (b) – logarithmic scale

Figs. 4a and 4b show the evolution of the radiative and non-radiative recombination rates with the In content. At 300K, a sharp increase in both recombination rates is observed when In content increases from 0.2 to 0.3. This can be attributed to the difficulty for the photogenerated carriers to escape from the absorption layer [14]

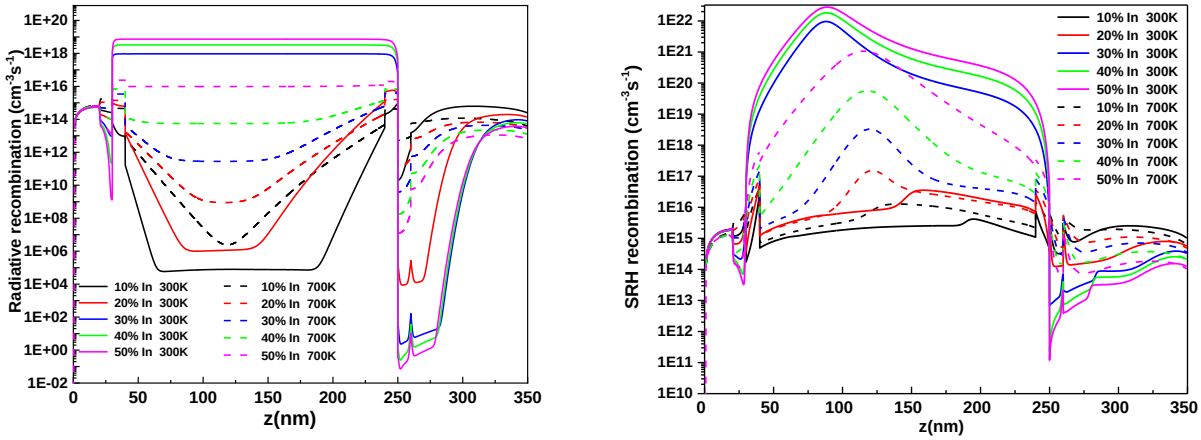

(a) (b)

Fig. 4: Recombination dependence upon temperature and Indium composition: (a) radiative recombination, (b) SRH recombination

The thermionic emission mechanism is strongly dependent on temperature (Eqs. 13 and 14). This effect is clearly seen on the energy bandgap diagrams of Fig 2a-e. For temperature as high as 700K, it can be noticed that the decrease of the electric field in the intrinsic layer when In content increases is mainly due to the decrease of the absorber bandgap and to the concomitant increases of the band offsets. Even for x=0.5, the electric field remains high enough to transport the carriers to the electrodes. This is also clearly seen in Fig. 3. Contrary to what it is observed at 300K, when In content increases from 10 to 30% at 500K and 700K, the current increases by a factor of around 5. This indicates that the additional photogenerated carriers due to the wider spectrum range covered by the decrease of the bandgap are well collected to the electrodes and can contribute to the photocurrent. Moreover, when regarding the evolution of the photocurrent with temperature for 0.1 In content, the increase is moderate and only due to the small reduction of the bandgap with temperature, this is in agreement with the low band offsets for such In composition which does not hinder the carrier transport at 300K. On the contrary, for an In content of 0.3, a strong increase of the photocurrent is observed when the temperature increases from 300K to 500K, indicating that for this composition, the carriers can surmounted the band offsets by thermionic effect at 500K but not at 300K.

However, the benefit of this expected photocurrent increase with temperature on the conversion efficiency is counterbalanced by the reduction of the V_{oc}, which is mainly caused by the increase of the dark current (linked with the increase of the intrinsic carrier concentration) as illustrated in Fig. 3b for both In compositions.

Contrary to what have been discussed previously concerning the recombination rates at 300K, the radiative and non-radiative recombinations at 700K increase regularly by around two orders and one order of magnitude respectively when the In content increases by step of 0.1, in agreement with the associated decrease of the bandgap (Figs. 4a and 4b) and their dependence proportional to Eg and Eg/2 respectively (Eqs. 9 and 10).

The carrier escape mechanism of thermionic emission with temperature can be evidenced by applying a reverse bias voltage as illustrated in Fig. 5a-b for an In composition of 0.5. In this figure J_{ph} indicates the theoretical available photocurrent [15]. It can be seen that this limit is reached at 0Volt for a temperature of 650K and at a "knee voltage" of -2V for a temperature of 600K. At higher temperature, the photocurrent is dominated by the dark current. At temperature lower than 650K, J_{sc} drastically decreases (Fig. 5b). This extended figure illustrates also the degradation of the fill factor when the temperature increases.

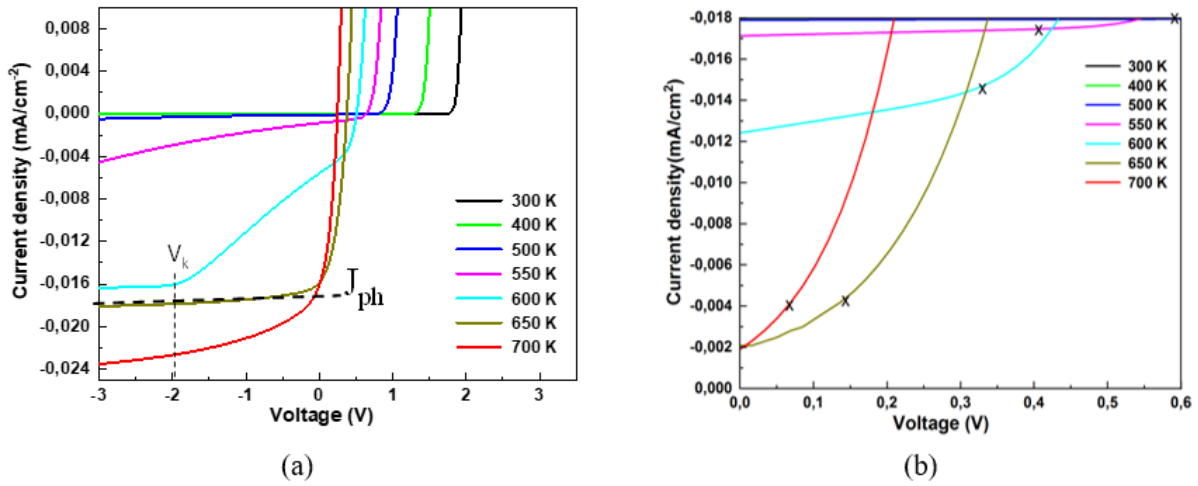

Fig. 5 : Photocurrent versus voltage characteristics for GaN/InGaN/GaN solar cell for various temperatures (x_{In}=0.5): (a) evidence of thermionic current contribution increase with temperature (The theoretical available photocurrent J_{ph} slightly increases from 1.53×10^{-2} mA/cm^2 at 400K to 1.68×10^{-2}mA/cm^2 at 700K (@ x_{In}=0.5); (b) zoom of PV quadrant: evidence of the impact of the thermionic current on the fill factor ($FF = \frac{J_{max}\,V_{max}}{J_{sc}\,V_{oc}}$), the crosses marked on the graph indicate the position of P_{max}.

The evolution of the double heterojunction solar cell parameters with temperature shows that due to the band offsets and thermal escaping mechanism of the photogenerated carriers, the maximum conversion efficiency conjointly depends on the In composition and temperature. To illustrate this, cartographies of the different parameters of the DHJ solar cells are plotted as a function of In content and temperature (Figs. 6a-6d).

For a fixed In composition, increasing the temperature leads to an increase of the Jsc up to the theoretical available photocurrent value. The transition between low and high Jsc levels is as marked and shifted towards high temperature as the In content is high. For a fixed

temperature, Jsc increases with In composition as the saturation photocurrent increases due to the extended absorption of the solar spectrum. However Jsc reaches a peak value due to the counterbalanced effect of band offset increase, the maximum Jsc value is reached for higher In content as the temperature increases. Voc variation varies more continuously with temperature and In content. Voc decreases with temperature due to the increase of the dark current and it decreases with the In content due to the reduction of the energy bandgap. The rollover phenomena observed in FF with temperature for fixed In content and with In content for fixed temperature can be ascribed to the trade-off between carrier escape and recombination as already proposed by Huang et al. [45]. The minimum of the fill factor is reached for the transition temperature at which only a part of the photogenerated carriers can overcome the potential barrier by thermionic effect to be collected to the electrodes, the other part being lost by recombination in the absorber. Degradation of the FF at very high temperature is related to the loss of photovoltaic effect due to high dark current and intrinsic carrier concentration.

On Fig. 6d, the conversion efficiency of the DHJ solar cell is found to reach a maximum for a given In content-working temperature pair. With the present simulation conditions, a maximum of 5% is obtained for an In content of 0.3 at 500K. When the In content increases, the position of the efficiency maximum is shifted towards the high temperatures, combining the need of higher temperature to surmount higher band offset and the decreasing efficiency with temperature commonly observed on conventional Si solar cells, due to Voc decrease. This result demonstrates that GaN/InGaN/GaN solar cells are suitable devices for high temperature operations but trade-off has to be solved between the targeted working temperature and the In content, and consequently the maximum expected efficiency.

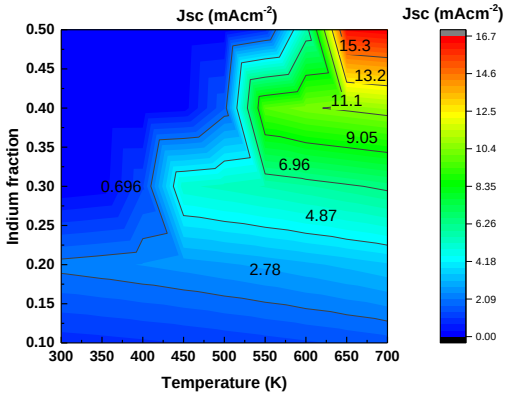

(a) Jsc

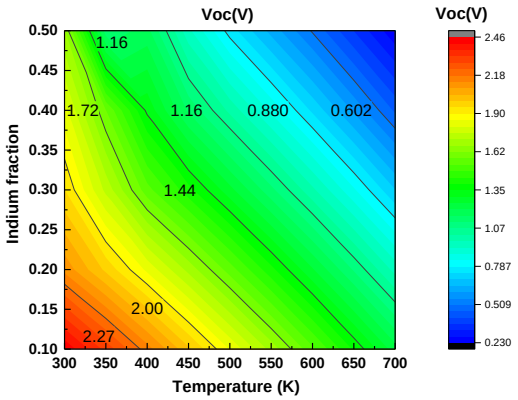

(b) Voc

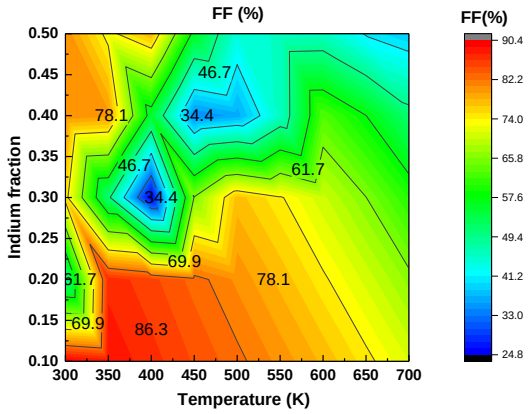

(c) Fill factor

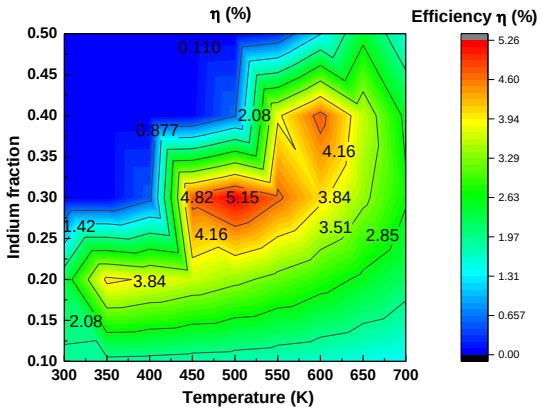

(d) Conversion efficiency

Fig. 6 : Cartographies showing the evolution of the solar cell parameters with temperature and In composition: (a) Jsc, (b) Voc, (c) FF, (d) Efficiency

3.2. Effect of the doping level of the n^+-GaN bottom layer

The doping level of the n^+-GaN bottom layer can change the potential barrier at the more limiting interface and therefore is a parameter which has to be carefully designed. The effect of the doping level of the bottom layer has already been studied at room temperature on InGaN quantum well solar cells [46,47] and it was shown that increasing the doping level of the GaN bottom layer leads to shift the "knee voltage" Vk (Fig. 5a) towards the positive voltages. Such effect is also illustrated on the band diagrams of the structure at 400K for an In content of 0.3 (Fig. 7). When the doping level of the bottom layer increases from 5×10^{17} cm^{-3} to $5\times10^{18}cm^{-3}$, the electric field is strongly enhanced, indicated that the photogenerated carriers are enable to go through the barrier and to be collected to the electrodes. This can also be linked with the marked reduction of the radiative and non-radiative recombinations observed (Fig. 8). Further increase of the doping level has no more additional effect.

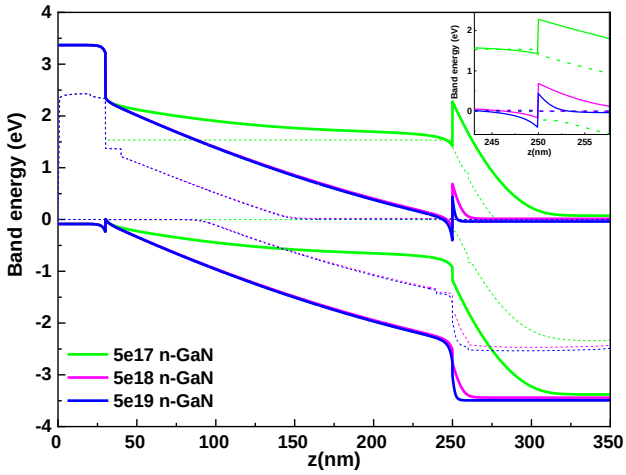

Figure 7. Effect of the doping concentration of the GaN bottom layer on the GaN/$In_xGa_{1-x}N$/GaN pin solar cell energy bandgap profile under zero bias at 400K and for x_{In}=30%.

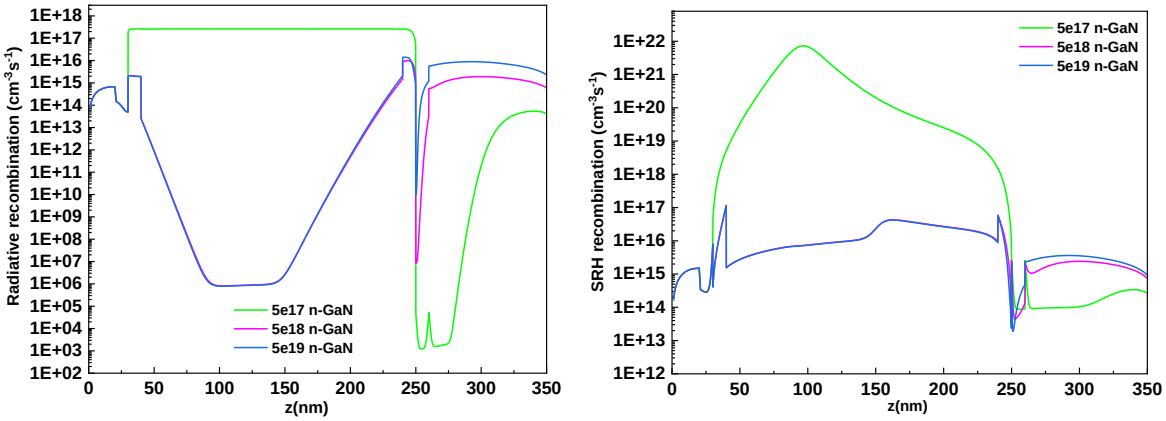

Figure 8: Effect of the doping concentration of the GaN bottom layer on the radiative and non-radiative recombination rates at 400K and for x_{In}=30%.

In order to follow the evolution of the solar cell parameters with the temperature and indium composition, the cartographies are replotted with the doping level of the bottom layer as the sole varying parameter (Fig. 9: $Nd_{GaN}=5\times10^{18}cm^{-3}$, Fig 10: $Nd_{GaN}=5\times10^{19}cm^{-3}$). When comparing Figs. 7b and 9b, as expected, V_{oc} is not significantly affected by the variation of n^+-GaN. On the contrary, as a consequence of the shift of the knee voltage, at fixed In composition, J_{sc} reaches the theoretical available photocurrent value at lower temperatures (Figs. 7a and 9a). This effect is obviously more evident as the In composition increases; at low In content, the potential barrier is too low to block the current. Due to the same reason, the main effect is visible on the fill factor, for which the lowest values of FF are shifted to the lower temperatures (Figs. 7c and 9c). As a result, the maximum efficiency slightly increases from 5.15 to 6.94%. The maximum is reached at almost the same temperature of 500K but for higher indium content (around 0.4 compared to 0.3 when n^+ increases from $5\times10^{17}cm^{-3}$ to $5\times10^{18}cm^{-3}$) (Figs. 7d and 9d). It can also be noticed that the efficiency increases for almost all configurations.

When the doping concentration of the bottom layer further increases up to $5\times10^{19}cm^{-3}$, Voc still remains unchanged (Fig. 10b). From Fig 10a, it can be noticed that Jsc at fixed In content is no more dependent on temperature, even for high In composition. Just a slight decrease with increasing temperature is noted in relation with the decrease of the bandgap, as observed on conventional solar cells. No more additional degradation due to the potential barrier is observed. From the inset of Fig.7, it is worth to note that when the concentration of the GaN layer increases, carrier confinement on the absorber side increases, resulting in an apparent reduction of the potential barrier at the interface[48,49]. The efficiency maximum increases to 12,2% and its position is shifted toward the higher Indium contents and lower temperatures. This means that the choice of the working temperature is determinant in the whole optimization of the structure design.

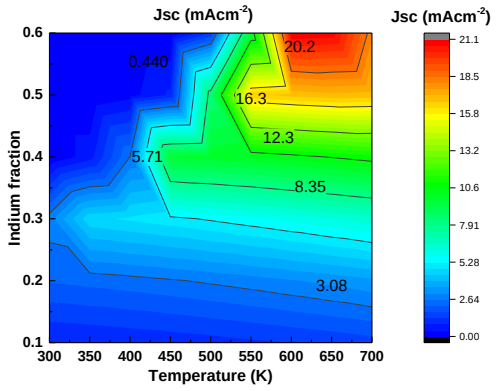

(a) Jsc

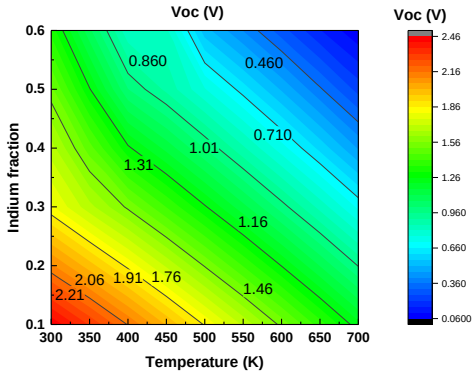

(b) Voc

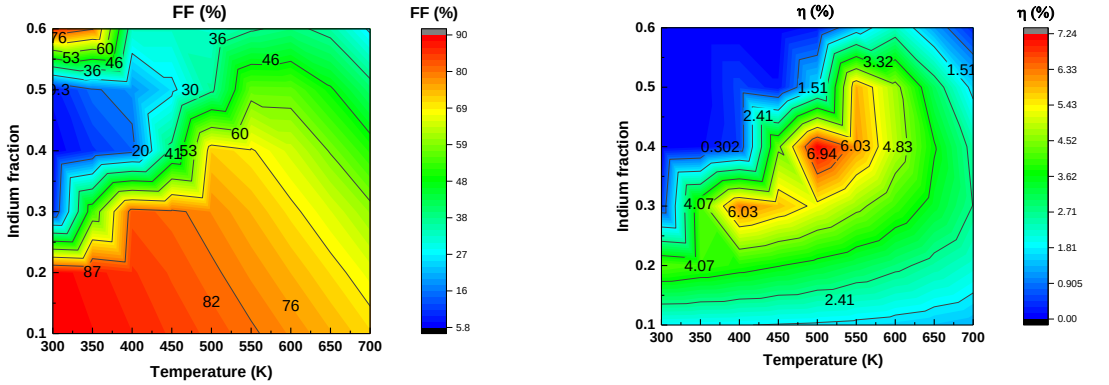

(c) Fill Factor (d) Conversion efficiency

Figure 9. Cartographies showing the evolution of the solar cell parameters with temperature and In composition for a doping level of the GaN bottom layer of $5\times10^{18}cm^{-3}$: (a) Jsc, (b) Voc, (c) FF, (d) Efficiency .

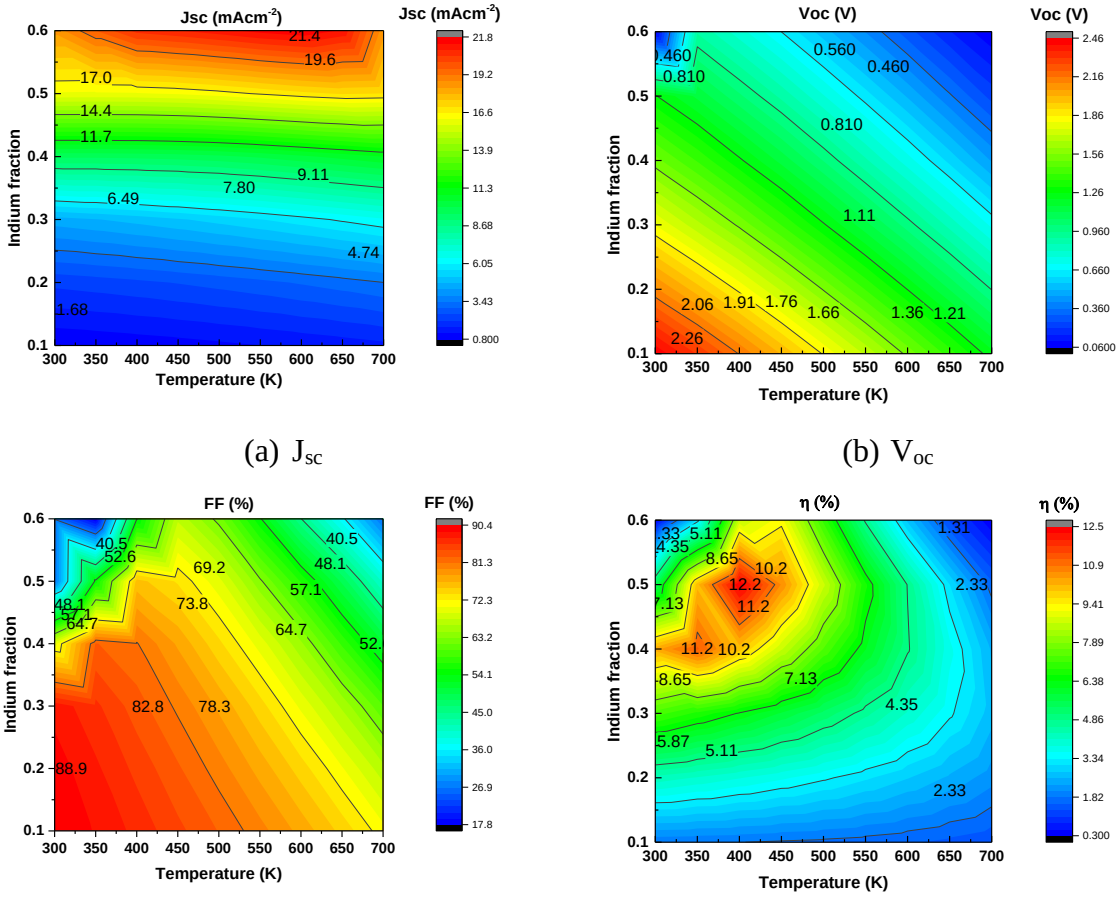

(a) J_{sc} (b) V_{oc}

(c) Fill factor (d) Conversion efficiency

Figure 10: Cartographies showing the evolution of the solar cell parameters with temperature and In composition for a doping level of the GaN bottom layer of $5\times10^{19}cm^{-3}$: (a) Jsc, (b) Voc, (c) FF, (d) Efficiency.

3.3. Effect of the density of non-radiative centers

As shown by eq. 18, the carrier lifetime results from competition between carrier escape mechanism and carrier recombination. From this point, it is interesting to evaluate the impact of the concentration of non-radiative centers on the conversion efficiency. On Fig. 11a, the proportional dependence of SRH recombination rate with the concentration of non-radiative centers is illustrated. The consequence of the reduction of the SRH recombination rate on the conversion efficiency is shown on Fig. 11b for two configurations close to optimal cases. For the lowest SRH center densities, when the SRH recombination rate is no more a limiting parameter, the conversion efficiency can reach up to 9% at 500K for 0.35 In content and up to 17% at 400K for 0.5 In content. On the contrary, a degraded quality of the absorber has a detrimental effect on the efficiency.

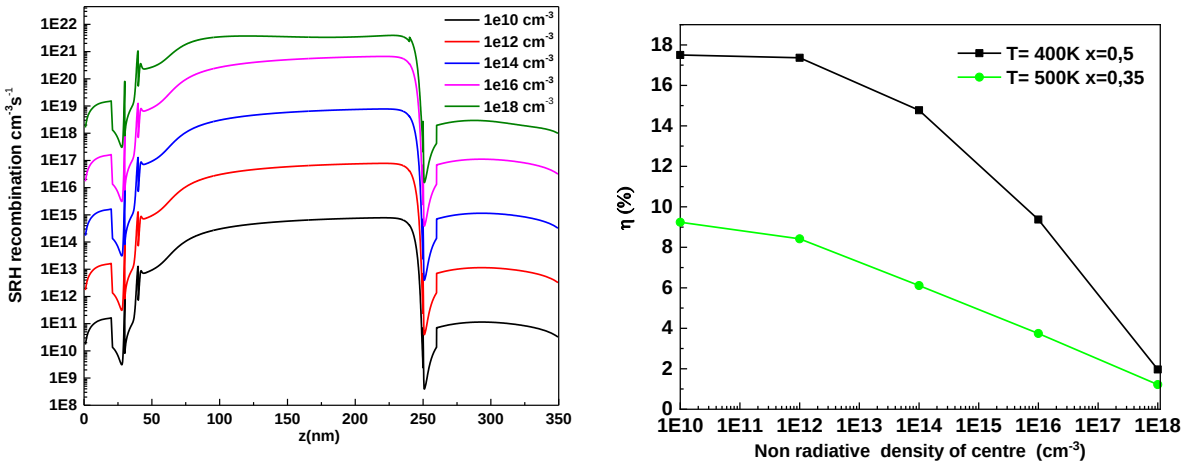

(a) (b)

Figure 11: Effect of non-radiative center density: (a) on the SRH recombination rate: x_{In}=0.5 T= 400K, $n^{+}_{GaN}=5\times10^{19}$ cm^{-3} , (b) on the conversion efficiency for two conditions : x_{In}=0.5 T= 400K, $n^{+}_{GaN}=5\times10^{19}$ cm^{-3} and x_{In}=0.35, T= 500K, $n^{+}_{GaN}=5\times10^{18}$ cm^{-3}

4. Conclusion

Numerical simulations taking into account the temperature dependence of the main physical parameters of GaN/InGaN/GaN solar cells have been carried out for high temperature applications. For DHJ structures, the compromise at room temperature is between reducing the bandgap to enlarge the covered solar spectrum and limiting the band offsets that hinter the collection of photogenerated carriers. When the operating temperature increases, the thermionic emission is favored and therefore the limiting effect of the band offsets is less and less critical. However in the same time, the strong increase of the intrinsic carrier concentration with temperature becomes a more and more limiting parameter by causing a rapid increase of the dark current and therefore a rapid reduction of Voc. So, wider bandgap absorbers are needed for higher working temperatures, resulting in lower conversion efficiencies. The optimized structure design is therefore primarily depending on the targeted working temperature, which firstly determines the bandgap of the absorber and consequently the resulting expected efficiency. Intrinsically, DJH InGaN/GaN solar cells are found to be adapted devices for very high temperature applications, requiring nevertheless a high material quality to reduce recombinations related to bulk and interface traps and a high quality of contact electrodes.

Acknowledgements

The authors extend their appreciation to the Deanship of Scientific Research at King Khalid University for funding this work through a research groups program under Grant Number R.G.P.2/203/42.

References:

[1] D. Merritt, S. Houlihan, R.P. Raffaelle, G.A. Landis, Wide bandgap space solar cells, 31st Photovoltaic Specialists conference, Lake Buena Vista Florida, (2005) 552, https://doi.org/10.1109/PVSC.2005.1488190.

[2] G. Moses, X. Huang, Y. Zhao, M. Auf der Maur, E.A. Katz, J. M. Gordon, InGaN/GaN multi-quantum well solar cells under high solar concentration and elevated temperatures for hybrid solar thermal-photovoltaic power plants, , Prog. Photovolt. Res. Appl., 28 (2020) 1167, ,https://doi.org/10.1002/pip.3326.

[3] J.J. Williams, H. McFavilen, A.M. Fischer, D. Ding, S. Young, E. Vadiee, F.A. Ponce, C. Arena, C.B. Honsverg, S.M. Goodnick, Refractory InxGa1-xN solar cells for high temperature applications, IEEE J. Photovoltaics 7(6) (2017) 1646, http://dx.doi.org/10.1109/JPHOTOV.2017.2756057.

[4] J.C.C. Fan, Theoretical temperature dependence of solar cell parameters, , solar cells, 17 (1986) 309, ,https://doi.org/10.1016/0379-6787(86)90020-7.

[5] M.G. Green, General temperature dependence of solar cell performance and implications for device modelling,, Prog. Photovolt: Res. Appl, 11 (2003) 333, https://doi.org/10.1002/pip.496.

[6] A. Landis, D. Meritt, R.P. Raffaelle, D. Scheiman,, High-temperature solar cell development, EuPVSEC, (2005) 241,

[7] C.J. Neufeld, N.G.Toledo, S.C. Cruz, M. Iza, S.P. DenBaars, U.K. Mishra,, High quantum efficiency InGaN/GaN solar cells with 2.95eV bandgap, Appl. Phys. Lett., 93 (2008) 143502, https://doi.org/10.1063/1.2988894.

[8] G. Bhuiyan, K. Sugita, A. Hashimoto, A. Yamamoto, InGaN Solar Cells: Present state of the art and important challenges, IEEE. J. Photov., 2 (2012) 276, http://10.1109/JPHOTOV.2012.2193384.

[9] X.M.Cai, S.-W. Zeng, B.-P. Zhang, Fabriation and characterization of InGaN p-i-n homojunction soar cell, Appl. phys.Lett/, 95 (2009) 173504.

[10] O.Jani, I. Ferguson, design and characterization of GaN/InGaN solar cells, applied physics letters, 91 (2007) 132117,http://dx.doi.org/10.1063/1.2793180.

[11] X. Zheng, R.-H. Horng, D.-S. Wuu, M.-T. Chu, W.-Y. Liao, M.-H. Wu, R.-M. Lin, Y.-C. Lu, High-quality InGaN/GaN heterojunctions and their photovoltaic effects, , Appl. Phys. Lett, , 9 (2008.) 261108 https://doi.org/10.1063/1.3056628.

[12] X. Cai, Y.Wang, B. Chen, M.-M. Liang, W.J. Liu, J.-Y. Zhang, X.-Q. Lv, L.Y. Ying, B.-P. Zhang, Investigation of InGaN p-i-n Homojunction and Heterojunction Solar Cells, IEEE Photonics Technol. Lett., 25 (2013) 59, https://doi.org/10.1109/LPT.2012.2227702.

[13] C.A.M. Fabien, A Maros, C.B. Honsberg, W.A. Doolittle, , III-Nitride double heterojunction solar cells with high In-content InGaN absorbing layers: comparison of large-area and small-area devices, IEEE J. Photovolt., 6(2) (2016) 460, https://doi.org/10.1109/JPHOTOV.2015.2504790.

[14] Y. K. Kuo, J. Y. Chang, Y.H. Shih, Numerical study of the effects of hetero-interfaces, polarization charges, and step-graded interlayers on the photovoltaic properties of (0001) face GaN/InGaN p-i-n solar cell, IEEE Journal of Quantum Electronics, 48 (2012) 367, https://doi.org/10.1109/JQE.2011.2181972.

[15] Silvaco data system Inc, Atlas user's manual, jan 31, 2017.

[16] I. Vurgaftman, J.R. Meyer, Band parameters for nitrogen-containing semiconductors, J. Appl. Phys. 94(6) (2003) 3675.

[17] W. Walukiewicz, S.X. Li, J. Wu, K.M. Yu, J.W. Ager III, E.E. Haller, H. Lu, W. J. Schaff, Optical properties and electronic structure of InN and In-rich group III-nitride alloys, J. Crys. Growth 269 (2004) 119.

[18] I. Gorczyca, S.P. Lepkowski, T. Suski, N.E. Christensen, A. Svane, Influence of indium clustering on the band structure of semiconducting ternary and quaternary nitride alloys, Phys. Rev. B 80 (2009) 075202.

[19] E. Sakalauskas, Ö. Tuna, A. Kraus, H. Bremers, U. Rossow, C. Giesen, M. Heuken, A. Hangleiter, G. Gobsch, R. Goldhahn, Dielectric function and bowing parameters of InGaN alloys, Phys. Stat. Sol. 249 (2012) 485,

[20] J.-Y. Chang, B.-T. Liou, H.-W. Lin, Y.-H. Shih, S.-H. Chang, Y.-K. Kuo, Numerical investigation on the enhanced carrier collection efficiency of GA-face GaN/InGaN p-i-n solar cells with polarization compensation interlayers, Optics Lett. 36(17) (2011) 3500.
[21] D.M. Caughey, R.E. Thomas, Carrier mobilities in silicon empirically related to doping and field, Proc. IEEE, 52 (1967) 2192.
[22] F. Schwierz, An electron mobility model for wurtzite GaN, Solid-State Electron., 49 (2005) 889, https://doi.org/10.1016/j.sse.2005.03.006.
[23] M. Farahmand, C. Garetto, E. Bellotti, K. F. Brennnan, M. Goano, E. Ghillino, G. Ghione, J. D. Albrecht, P.P Ruben, Monte Carlo simulation of electron transport in the III-Nitride wurtzite phase materials systems: binaries and ternaries, Trans. Electron. Dev. , 48 (3) (2001,) 535, https://doi.org/10.1109/16.906448.
[24] S. Wang, H. Liu, Q. Chen, H. Zhang, An analytical model of low field and high field electron mobility in wurtzite indium nitride, J. Mater. Sci.: Mater. Electron. , 27 (2016) 11353.
[25] M. Horita, S. Takashima, R. Tanaka, H. Matsuyama, K. Ueno, M. Edo, T. Takahashi, M. Shimizu, J. Suda, Jpn. J. Appl. Phys. 56 (2017) 031001.
[26] N. Ma, X.Q. Wang, S. T. Liu, G. Chen, J. H. Pan, L. Feng, F. J. Xu, N. Tang, B. Shen, Hole mobility in wurtzite InN, Appl. Phys. Lett. 98 (2011) 192114.
[27] G.F. Brown, J.W. Ager III, W. Walukiewicz, J. Wu,, Finite element simulations of compositionally graded InGaN solar cells, , Sol. Energy Mater. Sol. Cells, 94 (2010) 478, https://doi.org/10.1016/j.solmat.2009.11.010
[28] A. Adaine, S.O.S. Hamady, N. Fressengeas, Simulation study of a new InGaN p-layer free Schotky based solar cell, Superlatt. Microstruct., 96 (2016) 121, https://doi.org/10.1016/j.spmi.2016.05.020.
[29] S. Adachi, Refractive indices of II-V compounds: Key properties of InGaAsP relevant to device design, J. Appl. Phys. 53(8) (1982) 5863.
[30] S.N. Alam, V.Z. Zubialevich, B. Ghafary, P.J. Parbrook,, Bandgap and refractive index estimates of InAlN and related nitrides across their full composition ranges, Sci. Rep., 10 (2020) 1620, ,http://dx.doi.org/10.1038/s41598-020-73160-7
[31] S.F. Chichibu, K. Hasu, Y. Ishikawa, M. Tashiro, H. Namita, S. Nagao, K. Fujito, A. Uedono, Time-resolved photoluminescence, positron annihilation, and $Al_{0.23}Ga_{0.77}N$/GaN heterostructure growth studies on low defect density polar and nonpolar freestanding GaN substrate grown by hydride vapor phase epitaxy, J. Appl. Phys. 111 (2012) 103518.
[32] K. Kawakami, T. Nakano, A.A. Yamaguchi, Analysis of radiative and non-radiative lifetimes in GaN using accurate internal-quantum-efficiency values estimated by simultaneous photoluminescence and photo-acoustic measurements, Proc. SPIE, 9748 (2016) 97480S.
[33] S.F. Chichibu, K. Shima, K. Kojima, S. Takashima, M. Edo, K. Ueno, S. Ishabashi, A. Uedono, Large electron capture-cross-section of the major nonradiative recombination centers in Mg-dope GaN epilayers grown on a GaN substrate, Appl. Phys. Lett., 112 211901 2018.
[34] S.F. Chichibu, A. Uedono, K. Kojima, H. Ikeda, K. Fujito, S. Takashima, M. Edo, K. Ueno, S. Ishabashi, The origins and properties of intrinsic nonradiative recombination centers in wide bandgap GaN and AlGaN, J. Appl. Phys. 123, 161413 2018.
[35] X. Wang, S.-B. Che, Y. Ishitani, A. Yoshikawa, Hole mobility in Mg-doped p-type InN films, Appl. Phys. Lett., 92 (2008) 132108.
[36] V.M. Polyakov, F. Schwierz, Nonparabolicity effect on bulk transport properties in wurtzite InN, J. Appl. Phys., 99 (2006) 113705.
[37] K. Yang, J.R. East, G. I. Haddad, Numerical modeling of abrupt heterojunction using a thermionic-field emission boundary condition, Solid-State Electron. 36 (1993) 321.
[38] M.J. Wang, B. Shen, F.J. Xu, Y. Wang, J. Xu, S. Huang, Z.J. Yang, K. Xu, G.Y. Zhang, High temperature dependence of the density of two-dimensional electron gas in $Al_{0.18G}Ga_{0.82}N$/GaN heterostructures, Appl. Phys. A 88 (2007) 715.
[39] W.Götz, N.M. Johnson, C. Chen, H. Liu, C. Kuo, W. Imler, Activation energies of Si donors in GaN, Appl. Phys. Lett., 68(22) 1996, 3144.
[40] W. Götz, R.S. Kern, C.H. Chen, H. Liu, D.A. Steigerwald, R.M. Fletcher, Hall-effect characterization of III-V nitride semiconductors for high efficiency light emitting diodes, Mater. Sci. Eng. B59 (1999) 211.
[41] P. Kozodoy, H. Xing, S.P. DenBaars, U.K. Mishra, A. Saxler, R. Perrin, S. Elhamri, W.C. Mitchel, Heavy doped effects in Mg-doped GaN, J. Appl. Phys. 87 4 2000.

[42] M. Nawaz, A. Ahmad, A TCAD-based modeling of GaN/InGaN/Si solar cells, Semicond. Sci. Technol. 27 (2012) 035019.
[43] K. Wang, Q. Wang, J. Chu, H. Xiao, X. Wang, Z. Wang, Roles of polarization effects in InGaN/GaN solar cells and comparison of p-i-n and n-i-p structures, Optics Express, 26 (2018) A946.
[44] J.R. Lang, N.G. Young, R.M. Farrell, Y.-R. Wu, J.S. Speck, Carrier escape mechanism dependence on barrier thickness and temperature in InGaN quantum well solar cells, Appl. Phys. Lett. 101 (2012) 181105.
[45] X. Huang, W. Li, H. Fu, D. Li, C. Zhang, H. Chen, Y. Fang, K. Fu, S. P. DenBaars, S. Nakamura, S. M. Goodnick, C.-Z. Ning, S. Fan, Y. Zhao, High-temperature polarization-free III-Nitride solar cells with self-cooling effects, ACS Photonics 6 (2019) 2096.
[46] R.M. Farrell, C.J. Neufeld, S.C. Cruz, N.G. Young , M. Iza, J. R. Lang, Y.-L. Hu, D. Simeonov, N. Singh, E.E. Perl, T. Lin, N.G. Toledo, S. Keller, D.J. Friedman, J. E. Bowers, S. Nakamura, S.P. DenBaars, J.S. Speck, U.K. Mishra, InGaN-based solar cells for ultrahigh efficiency multijunction solar cell applications, UC Solar Research Symposium, 2011, Merced, Ca (USA).
[47] C.J. Neufeld, S.C. Cruz, R.M. Farrell, M. Iza, J. R. Lang, S. Keller, S. Nakamura, S.P. DenBaars, J.S. Speck, U.K. Mishra R.M. Farrell, C.J. Neufeld, S.C. Cruz, N.G. Young , M. Iza, J. R. Lang, Y.-L. Hu, D. Simeonov, N. Singh, E.E. Perl, T. Lin, N.G. Toledo, S. Keller, D.J. Friedman, J. E. Bowers, S. Nakamura, S.P. DenBaars, J.S. Speck, U.K. Mishra, Effect of doping and polarization on carrier collection in InGaN quantum well solar cells, Appl. Phys. Lett., 98 (2011) 243507.
[48] B Chouchen, M H Gazzah, A Bajahzar and H. Belmabrouk, Numerical modeling of InGaN/GaN pi-n solar cells under temperature and hydrostatic pressure effects AIP Advances 9, (2019) 045313
[49] B Chouchen, M H Gazzah, A Bajahzar and H. Belmabrouk, Numerical Modeling of the Electronic and Electrical Characteristics of InGaN/GaN-MQW Solar Cells Materials 12 (2019) 1241.